Biochemistry

 Volume 40, Number 24 June 19, 2001

Accelerated Publications

Molecular Structure of Dihydroorotase: A Paradigm for Catalysis through the Use of a Binuclear Metal Center[†,‡]

James B. Thoden,[§] George N. Phillips, Jr.,[§] Tamiko M. Neal,[||] Frank M. Raushel,*[,||] and Hazel M. Holden*[,§]

Department of Biochemistry, University of Wisconsin, Madison, Wisconsin 53706, and Department of Chemistry, P.O. Box 30012, Texas A&M University, College Station, Texas 77842-3012

Received April 4, 2001; Revised Manuscript Received May 2, 2001

ABSTRACT: Dihydroorotase plays a key role in pyrimidine biosynthesis by catalyzing the reversible interconversion of carbamoyl aspartate to dihydroorotate. Here we describe the three-dimensional structure of dihydroorotase from *Escherichia coli* determined and refined to 1.7 Å resolution. Each subunit of the homodimeric enzyme folds into a "TIM" barrel motif with eight strands of parallel β-sheet flanked on the outer surface by α-helices. Unexpectedly, each subunit contains a binuclear zinc center with the metal ions separated by ~3.6 Å. Lys 102, which is carboxylated, serves as a bridging ligand between the two cations. The more buried or α-metal ion in subunit I is surrounded by His 16, His 18, Lys 102, Asp 250, and a solvent molecule (most likely a hydroxide ion) in a trigonal bipyramidal arrangement. The β-metal ion, which is closer to the solvent, is tetrahedrally ligated by Lys 102, His 139, His 177, and the bridging hydroxide. L-Dihydroorotate is observed bound to subunit I, with its carbonyl oxygen, O4, lying 2.9 Å from the β-metal ion. Important interactions for positioning dihydroorotate into the active site include a salt bridge with the guanidinium group of Arg 20 and various additional electrostatic interactions with both protein backbone and side chain atoms. Strikingly, in subunit II, carbamoyl L-aspartate is observed binding near the binuclear metal center with its carboxylate side chain ligating the two metals and thus displacing the bridging hydroxide ion. From the three-dimensional structures of the enzyme-bound substrate and product, it has been possible to propose a unique catalytic mechanism for dihydroorotase. In the direction of dihydroorotate hydrolysis, the bridging hydroxide attacks the *re*-face of dihydroorotate with general base assistance by Asp 250. The carbonyl group is polarized for nucleophilic attack by the bridging hydroxide through a direct interaction with the β-metal ion. During the cyclization of carbamoyl aspartate, Asp 250 initiates the reaction by abstracting a proton from N3 of the substrate. The side chain carboxylate of carbamoyl aspartate is polarized through a direct electrostatic interaction with the binuclear metal center. The ensuing tetrahedral intermediate collapses with C−O bond cleavage and expulsion of the hydroxide which then bridges the binuclear metal center.

Dihydroorotase (DHO)[1] is a zinc metalloenzyme that catalyzes the reversible cyclization of carbamoyl L-aspartate to L-dihydroorotate in the biosynthetic pathway for the assembly of pyrimidine nucleotides (Scheme 1). In higher organisms, this enzyme is found within a large polyfunctional protein (CAD) that also contains the catalytic activities for

[†] This research was supported in part by NIH Grants GM-33894 (to F.M.R.) and GM-55513 (to H.M.H.).

[‡] X-ray coordinates have been deposited in the Research Collaboratory for Structural Bioinformatics, Rutgers University, New Brunswick, NJ (XXXX).

* To whom correspondence should be addressed. E-mail: Hazel_Holden@biochem.wisc.edu or raushel@tamu.edu. Fax: (608) 262-1319. Phone: (608) 262-4988.

[§] University of Wisconsin.

[||] Texas A&M University.

10.1021/bi010682i CCC: $20.00
Published on Web 05/25/2001

Scheme 1

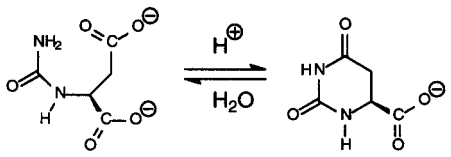

carbamoyl phosphate synthetase and aspartate transcarbamoylase. In bacteria such as *Escherichia coli*, however, DHO is a homodimeric and monofunctional enzyme with a molecular weight of ~76600 (*1*).

The catalytic mechanism of action for DHO has been probed by a number of research groups through the use of pH−rate profiles (*2*), site-directed mutagenesis techniques (*3*, *4*), and the preparation of metal-substituted variants (*5*, *6*). The hydrolytic cleavage of dihydroorotate is favored at high pH, while the cyclization of carbamoyl aspartate is optimal at pH ~7 (*2*). Strikingly, the native zinc ions have been substituted with Co^{2+}, Mn^{2+}, and Cd^{2+} with retention of significant catalytic activity (*5*, *6*). Structural and/or catalytic roles for histidine residues have been implicated by the suppression of enzymatic activity with diethylpyrocarbonate (*2*, *3*). Additionally, published amino acid sequence alignments of DHO from various species have identified a number of conserved residues that likely serve as ligands to the metal(s), function as general acids and/or bases, and/or provide electrostatic interactions with the substrate (*6*). In particular, Christopherson (*3*, *8*) has proposed a model for the active site of DHO from hamster that is reminiscent of the active site found in carbonic anhydrase. In this model, three conserved histidine residues (His 16, His 18, and His 177) are direct metal ligands to the single divalent cation while Arg 20, Asp 250, and His 139 function as general acid−base catalysts and/or in the binding of the substrates to the active site (numbering refers to that of the *E. coli* enzyme). Evans (*4*) has proposed a similar model for the active site of DHO from the same organism.

Interestingly, recent amino acid sequence alignments by Holm and Sander have clearly implicated DHO as belonging to the amidohydrolase superfamily (*9*). This superfamily contains a group of proteins that catalyze a diverse set of hydrolytic reactions at carbon and phosphorus centers. The superfamily has been divided into two subsets of enzymes. To date, the best-characterized members of the amidohydrolase superfamily include phosphotriesterase and urease that belong to one subset and adenosine deaminase that is grouped in the second subset. The active sites for phosphotriesterase and urease are very similar, with both containing binuclear metal centers (*10*, *11*). The two metal ions are bridged by a solvent hydroxide and a carbamate functional group formed by the carboxylation of the ϵ-amino group of a lysine side chain with CO_2. Other conserved direct metal ligands include an aspartate and a cluster of four histidine residues. Adenosine deaminase apparently binds a single divalent cation, however (*12*). There is thus an inherent plasticity in the number of divalent cations recruited to the active sites of enzymes belonging to this superfamily. The critical structural element for belonging to the first subset is the positioning of a carboxylated lysine residue that serves as one of the bridging ligands. Phosphotriesterase and urease each contain a lysine residue at this specific location, whereas the PTE homology protein from *E. coli* possesses a glutamate residue that serves to bridge the two divalent cations (*13*).

DHO was originally suggested to be a member of the second subset of the amidohydrolase superfamily in that it was believed to bind a single divalent cation (*9*). This proposal was supported by both the results of metal reconstitution studies and the apparent failure to identify a conserved lysine residue in amino acid sequence alignments (*7*, *9*). In this paper, we report the high-resolution X-ray structure of DHO from *E. coli*. Surprisingly, the active site clearly contains a binuclear metal center with the ϵ-amino group of Lys 102 carboxylated and serving as one of the two bridging ligands to the pair of zinc atoms. Additionally, the homodimeric protein within the asymmetric unit contains bound dihydroorotate in subunit I and carbamoyl aspartate in subunit II. The positioning of the catalytic residues relative to the substrate and product enables a novel reaction mechanism for DHO to be proposed, and indeed, this mechanism may be directly applicable to other members of the amidohydrolase superfamily containing binuclear metal centers.

MATERIALS AND METHODS

Crystallization and X-ray Data Collection. The protein employed for crystallization trials was purified according to procedures adapted from Washabaugh and Collins (*1*). The final protein sample (~8 mg/mL) was dialyzed into 10 mM HEPES (pH 7.0), 180 mM KCl, 10 mM *N*-carbamoyl-D,L-aspartate, and 5 mM DTT. Large single crystals were obtained by macroseeding into batch experiments at 4 °C using as the precipitant 6−9% poly(ethylene glycol) 3400, 100 mM MES (pH 6.0), 75 mM $MgCl_2$, and 150 mM KCl. The crystals achieved maximum dimensions of 1.0 mm × 0.3 mm × 0.3 mm in approximately 2−4 weeks and belonged to space group $P2_12_12_1$ with the following typical unit cell dimensions: $a = 51.6$ Å, $b = 78.8$ Å, and $c = 180.3$ Å. The asymmetric unit contained a dimer.

For preparation of a single heavy atom derivative, native crystals were transferred to solutions containing 15% poly(ethylene glycol) 3400, 100 mM MES (pH 6.0), 200 mM KCl, 75 mM $MgCl_2$, 5 mM *N*-carbamoyl-D,L-aspartate, and 1 mM iodoacetamide (to block reactive sulfhydryl groups) for 12 h. These crystals were then transferred to the same solution without the iodoacetamide to remove any excess modifying agent. Next the crystals were transferred to 15% poly(ethylene glycol) 3400, 100 mM MES (pH 6.0), 200 mM KCl, 75 mM $MgCl_2$, 5 mM *N*-carbamoyl-D,L-aspartate, and 2 mM $(NH_4)_2OsBr_6$ and allowed to equilibrate for 4 days. The crystals were then transferred to cryoprotectant solutions of a synthetic mother liquor containing 20% poly(ethylene glycol) 3400, 100 mM MES (pH 6.0), 400 mM KCl, 75 mM $MgCl_2$, 5 mM *N*-carbamoyl-D,L-aspartate, and 20% ethylene glycol. Each crystal was subsequently flash-cooled to −150 °C in a stream of nitrogen gas and subsequently stored under liquid nitrogen until synchrotron beam time became available. For collection of a high-resolution X-ray data set, crystals of the native enzyme were soaked for 2 days in 15% poly(ethylene glycol) 3400, 100 mM MES (pH 6.0), 200 mM

[1] Abbreviations: DHO, dihydroorotase; DTT, dithiothreitol; HEPES, *N*-(2-hydroxyethyl)piperazine-*N*′-2-ethanesulfonic acid; MES, 2-(*N*-morpholino)ethanesulfonic acid.

Table 1: X-ray Data Collection Statistics

	wavelength (Å)	resolution (Å)	no. of independent reflections	completeness (%)	redundancy	avg I/avg $\sigma(I)$	R_{sym}[a]
peak	1.14020	99.00−2.26	35229	99.8	7.2	59.4	6.4
		2.34−2.26[b]	3456	99.3	6.7	19.5	15.5
inflection	1.14050	99.00−2.26	35209	99.8	7.2	59.2	5.9
		2.34−2.26	3455	99.4	6.7	18.5	16.4
remote	1.09045	99.00−2.16	40196	99.8	7.2	58.3	5.4
		2.24−2.16	3956	99.1	6.7	15.1	19.8
native	1.03320	99.00−1.50	114211	97.7	6.2	41.1	5.4
		1.55−1.50	10107	87.5	3.0	2.3	24.7

[a] $R_{sym} = (\sum|I - \bar{I}|/\sum I) \times 100$. [b] Statistics for the highest-resolution bin.

KCl, 75 mM $MgCl_2$, and 50 mM *N*-carbamoyl-D,L-aspartate. These crystals were subsequently flash-cooled according to a procedure similar to that described for the osmium-containing crystals.

Both the high-resolution native and the heavy atom derivative X-ray data sets were collected on a 3 × 3 tiled "SBC2" CCD detector at the Structural Biology Center 19-ID Beamline (Advanced Photon Source, Argonne National Laboratory, Argonne, IL). The X-ray data were processed with HKL2000 and scaled with SCALEPACK (*14*). Relevant X-ray data collection statistics are presented in Table 1.

X-ray Structural Analyses. The structure of DHO was determined via MAD phasing with the single osmium derivative. Two osmium binding sites were identified by visual inspection of a Patterson map calculated on the basis of the anomalous differences to 2.8 Å resolution. The positions, occupancies, and temperature factors for these sites were refined with the software package SOLVE (*15*). Protein phases were calculated to 2.4 Å resolution with SOLVE. Density modification procedures were performed with the program RESOLVE (*16*) and led to an electron density map showing well-defined regions of α-helical structure and the position of the local 2-fold rotational axis relating the two subunits in the asymmetric unit. Molecular averaging about the local dyad with the program DM (*17*) resulted in a readily interpretable electron density map. The model generated from this electron density map was subjected to alternate cycles of least-squares refinement at 1.7 Å resolution with the software package TNT (*18*) and manual adjustment with the graphics program TURBO FRODO (*19*). Electron density maps were subsequently calculated with coefficients of the form $F_o - F_c$ and examined for solvents and other bound molecules. Surprisingly, these electron density maps revealed that L-dihydroorotate was bound in the active site for subunit I while *N*-carbamoyl-L-aspartate was located in the active site for subunit II as shown in panels a and b of Figure 1, respectively. Final refinement statistics are given in Table 2. Note that the *R*-factors listed in Table 2 are based on all measured X-ray data with no σ cutoffs applied.

A Ramachandran plot of all non-glycinyl ϕ and ψ angles indicates only three residues adopt dihedral angles well outside of the allowed regions. Two of these correspond to Arg 20 in both subunits ($\phi \sim 60°$, $\psi \sim -149°$). Arg 20 is located in the active site where its side chain guanidinium group forms a salt bridge with the α-carboxylate of dihydroorotate in subunit I or the α-carboxylate of carbamoyl aspartate in subunit II. The electron density for Arg 20 in both subunits is unambiguous. The other significant outlier in the Ramachandran plot is Asp 330 in subunit II ($\phi = 76°$, $\psi = -174°$). This residue is located in a reverse turn connecting two strands of antiparallel β-sheet at the C-terminus. Again, the electron density corresponding to this residue is well-ordered.

Table 2: Least-Squares Refinement Statistics

resolution limits (Å)	30.0−1.70
R-factor[a] (overall) (%)/no. of reflections	19.3/79036
R-factor (working) (%)/no. of reflections	19.1/71132
R-factor (free) (%)/no. of reflections	25.8/7904
no. protein atoms[b]	5447
no. of heteroatoms[c]	770
average *B* values (Å^2)	
protein	31.9
ligands	37.2
weighted root-mean-square deviations from ideality	
bond lengths (Å)	0.012
bond angles (deg)	2.15
trigonal planes (Å)	0.006
general planes (Å)	0.010
torsional angles[d] (deg)	17.1

[a] $R\text{-factor} = (\sum|F_o - F_c|/\sum|F_o|) \times 100$, where F_o is the observed structure factor amplitude and F_c is the calculated structure factor amplitude. [b] These include multiple conformations for R11, L25, Q60, N107, K131, V142, R155, R193, V245, R256, and Q301 in subunit I and R91, R155, and R193 in subunit II. [c] These include 731 water molecules, 4 zinc ions, 1 dihydroorotate, and 2 carbamoyl aspartates. [d] The torsional angles were not restrained during the refinement.

RESULTS AND DISCUSSION

Structure of DHO. DHO from *E. coli* functions as a dimer (*1*). A ribbon representation of the dimer is shown in Figure 2. The molecule has overall dimensions of 73 Å × 77 Å × 80 Å with the two active sites separated by approximately 25 Å. As can be seen, the subunit−subunit interface is fairly extensive and formed primarily by three loop regions contributed by each subunit: His 144−Arg 152, Arg 207−Arg 227, and Glu 260−Gly 264. The first two regions contain well-defined secondary structural elements. Specifically, the polypeptide chain from His 144 to Arg 152 folds into two type I turns, while the region defined by residues Arg 207−Arg 227 adopts an α-helical conformation followed by a type II turn and then two type I turns. The third loop region, from Glu 260 to Gly 264, adopts a random coil conformation. As calculated according to the method of Lee and Richards (*20*) with a 1.4 Å search probe, the surface area lost upon dimerization is ∼2300 Å^2. Key salt bridges that serve to stabilize the subunit−subunit interface occur between Asp 148 (subunit I) and Arg 207 (subunit II) and between Asp 151 (subunit I) and Arg 227 (subunit II) and the 2-fold related pairs. Additionally, the backbone carbonyl oxygen of Ile 147 and the peptidic nitrogen of Ile 149 (subunit I) form hydrogen bonds with the side chain carboxamide group of Asn 208 (subunit II). Apart from these

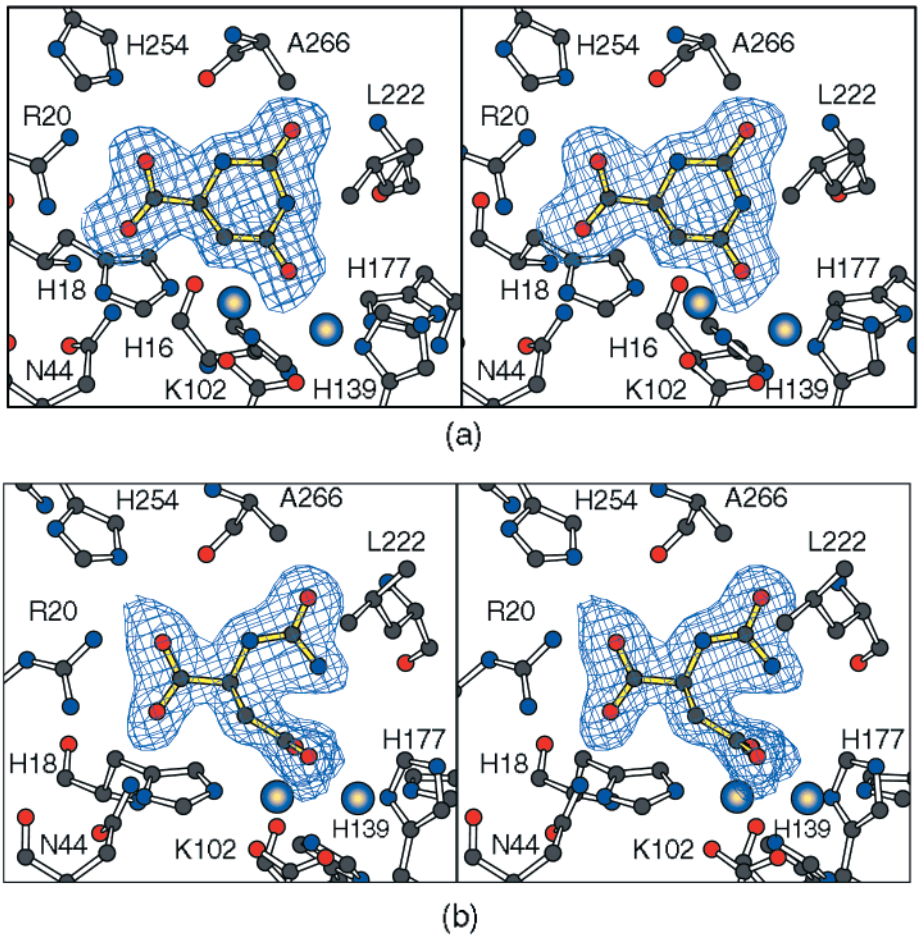

FIGURE 1: Electron density corresponding to bound dihydroorotate or carbamoyl aspartate in the dimer. All figures were prepared with the software package, MOLSCRIPT (*28*). The electron density maps displayed in panels a and b were contoured at 2σ and calculated with coefficients of the form $F_o - F_c$, where F_o was the native structure factor amplitude and F_c was the calculated structure factor amplitude. The dihydroorotate and carbamoyl aspartate molecules had not been built into the electron density map prior to the Fourier synthesis. Shown in panel a is the electron density observed in subunit I which clearly indicates the presence of dihydroorotate. The electron density in panel b shows the manner in which carbamoyl aspartate is accommodated in the active site.

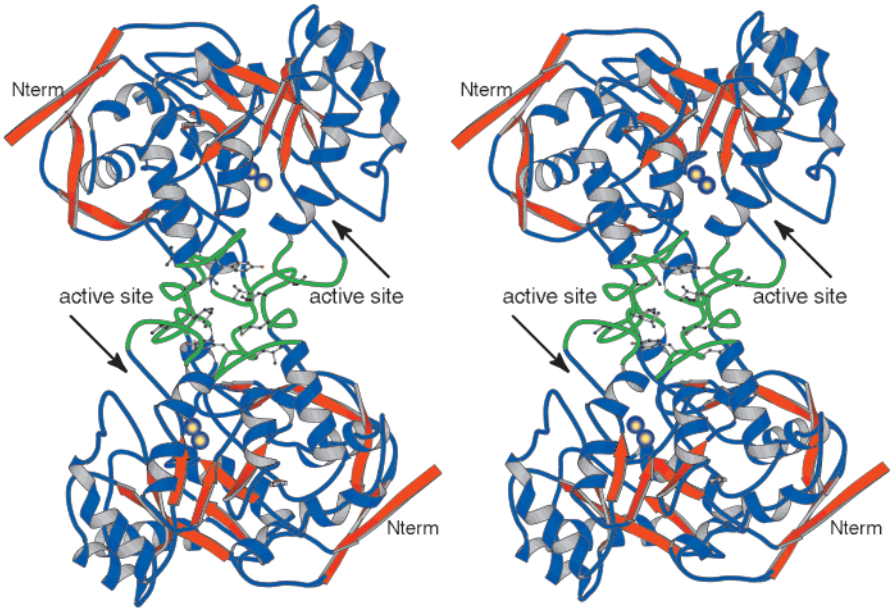

FIGURE 2: Ribbon representation of the DHO dimer. The strands of β-sheet are highlighted in red, and the loops forming the subunit−subunit interface are drawn in green. In addition to the core TIM barrel, the polypeptide chain folds into an additional five β-strands, three α-helices, and various type I, II, and III turns.

electrostatic interactions, the molecular interface is quite nonpolar with the side chains of Ile 149, Phe 150, Met 210, Leu 211, Val 212, Val 215, Tyr 220, Leu 222, and Leu 224 in subunit I and the symmetry-related residues in subunit II

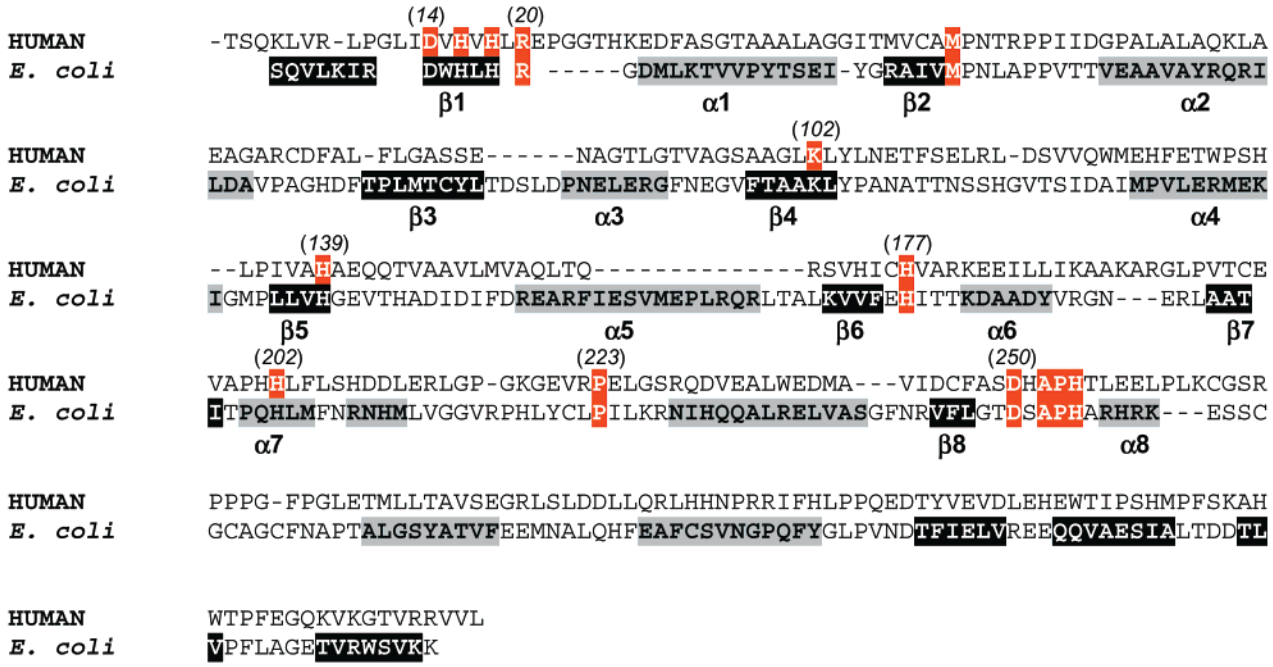

FIGURE 3: Amino acid sequence alignment between the DHO from *E. coli* and humans. The β-strands in the structure of the bacterial DHO are indicated by a black background with white letters, whereas the α-helices are indicated by a gray background with black letters. The fully conserved amino acids are designated by a red background with white letters. The residue numbers of the bacterial enzyme are indicated in parentheses.

forming a "sticky" patch. Indeed, there are very few water molecules located directly within the subunit−subunit interface. Other than the surface loop formed by residues Pro 105−Thr 117, the two subunits of the dimer are very similar such that their α-carbons superimposed with a root-mean-square deviation of 0.22 Å.

Not unexpectedly, and in light of previous suggestions that DHO belongs to the amidohydrolase superfamily of enzymes, each subunit of the dimer contains a "TIM" barrel motif with eight strands of parallel β-sheet flanked on the outer surface by α-helices. The eight strands forming the β-barrel are delineated by residues Asp 14−His 18, Arg 38−Val 41, Thr 73−Leu 80, Phe 98−Leu 103, Leu 136−His 139, Lys 172−Phe 175, Ala 195−Ile 198, and Val 245−Leu 247. These strands are connected to one another by a total of nine α-helices, ten type I turns, one type II turn, and four type III turns. In addition to the core of the TIM-barrel motif, there are five additional β-strands that form small regions of antiparallel sheet and that flank one side of the β-barrel. Each subunit has overall dimensions of approximately 51 Å × 51 Å × 54 Å. There are two *cis*-prolines per subunit, Pro 47 and Pro 223. Pro 47 is situated at the opening of the β-barrel, while Pro 223 is deeply embedded in the active site where the carbonyl oxygen of the preceding residue, namely, Leu 222, forms a hydrogen bond to N3 of dihydroorotate in subunit I or to N3 of carbamoyl aspartate in subunit II. The secondary structural assignments for the *E. coli* enzyme are summarized in the amino acid sequence alignment with human DHO in Figure 3.

Active Site Containing Bound Dihydroorotate. A closeup view of the active site for subunit I with bound dihydroorotate is shown in Figure 4a. There are seven water molecules located within 4.5 Å of the bound dihydroorotate. In addition, a water or hydroxide ion bridges the two zinc ions. Lys 102 is carboxylated and acts as the second bridging ligand in the binuclear metal center. The more buried or α-metal ion is bound in a distorted trigonal bipyramidal coordination sphere by His 16, His 18, Lys 102, Asp 250, and the bridging solvent with the side chains of Lys 102 and Asp 250 serving as the axial ligands. Angles formed between the ligands and the zinc in the equatorial plane range from 116° to 126°, while those between an axial ligand, the metal, and an equatorial ligand range from 79° to 104°. Both His 16 and His 18 are positioned in the first β-strand of the TIM barrel; Lys 102 is located on the fourth β-strand, and Asp 250 lies at the end of the last β-strand. His 139, His 177, Lys 102, and the bridging solvent surround the more solvent-exposed or β-metal in a distorted tetrahedral environment. His 139 is located in the fifth β-stand of the barrel, while His 177 sits at the end of the sixth strand. Angles between the ligands and the β-metal range from 94° to 105°. The two zinc ions are separated by 3.5 Å.

As can be seen in Figure 4a, O4 of dihydroorotate points toward the binuclear metal center and is situated at 2.9 Å from the β-metal and 2.7 Å from the bridging hydroxide. Likewise, N3 of dihydroorotate is in close contact with the bridging solvent (2.9 Å) and also lies within hydrogen bonding distance (3.1 Å) of the carbonyl oxygen of Leu 222. The peptidic NH of Leu 222 forms a hydrogen bond with O2 of dihydroorotate, while the backbone carbonyl group of Ala 266 lies within 3.0 Å of N1 of dihydroorotate. Those side chains serving to anchor the carboxylate group of dihydroorotate within the active site include Arg 20, Asn 44, and His 254. Interestingly, C4 and N3 of dihydroorotate are located at 2.8 and 3.7 Å from the bridging solvent and the carboxylate group of Asp 250, respectively, and indeed, this combination of solvent and side chain functional group may have important mechanistic implications as will be discussed below.

Active Site Containing Bound Carbamoyl Aspartate. A closeup view of the DHO active site with bound carbamoyl aspartate (subunit II) is shown in Figure 4b. In this case,

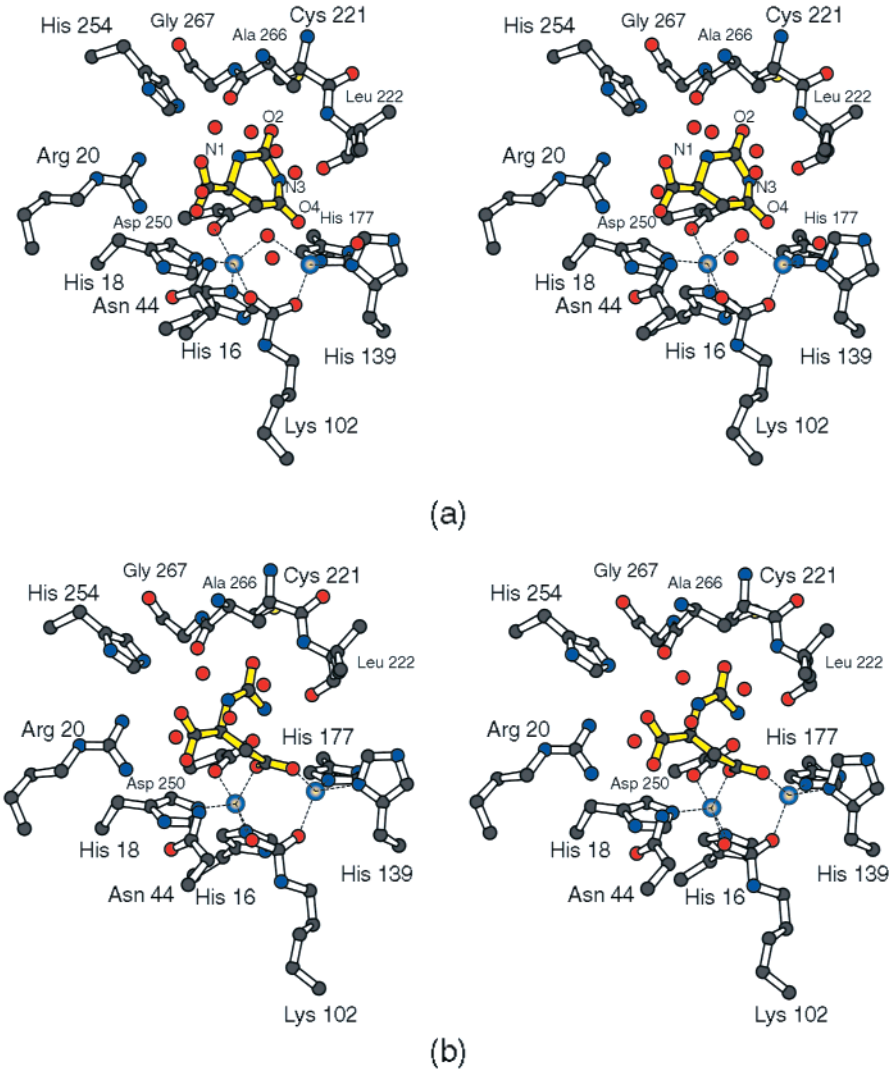

FIGURE 4: Closeup view of the active sites for DHO. Those atoms located within approximately 4.5 Å of dihydroorotate in subunit I are shown in panel a. The bound product is highlighted in yellow bonds, while the zincs are displayed in purple to yellow gradients. Dashed lines represent coordinate covalent bonds between the protein side chains (or solvent) and the metal ions. The numbering for the dihydroorotate corresponds to the standard system for pyrimidine rings. Those atoms located within approximately 4.5 Å of carbamoyl aspartate in subunit II are depicted in panel b. Note that the carboxylate side chain of carbamoyl aspartate displaces the bridging hydroxide from the binuclear metal center.

there are four ordered water molecules located within 4.5 Å of carbamoyl aspartate. Note that the bridging solvent of the binuclear metal center has been displaced by the side chain carboxylate of the substrate. The carbamoyl moiety of carbamoyl aspartate forms hydrogen bonds with the backbone NH and CO groups of Leu 222 (both at 2.7 Å), while the α-carboxylate group of the substrate is, again, bridged to the enzyme via a salt bridge with the guanidinium group of Arg 20 and hydrogen bonds with Asn 44 and His 254. Strikingly, N3 of carbamoyl aspartate is situated 3.0 Å from the carboxylate group of Asp 250. To form dihydroorotate, this nitrogen must be deprotonated prior to its intramolecular nucleophilic attack on the side chain carboxylate carbon of carbamoyl aspartate. As can be seen in Figure 4b, there are no other catalytic bases other than Asp 250 within the general vicinity of N3 of the substrate.

With respect to the binuclear metal center, the trigonal bipyramidal coordination geometry around the α-metal in subunit II is similar to that observed in subunit I with the only major difference being the replacement of the bridging hydroxide with a carboxylate oxygen. The distance between the carboxylate group of the substrate and the α-metal in subunit II (2.3 Å) is similar to that observed between the hydroxide and the α-metal in subunit I (2.0 Å). Bond angles between the equatorial ligands (Lys 102 and Asp 250) and the metal range in size from 106° to 133°, and those angles between the axial ligands, the metals, and the equatorial ligands range in size from 82° to 99°. The β-metal is tetrahedrally ligated by Lys 102, His 139, His 177, and the side chain carboxylate group of the substrate with angles ranging from 89° to 108°. In subunit I, the distance between the β-zinc and the hydroxide is 2.4 Å, while in subunit II, the distance between the structurally equivalent carboxylate oxygen and the β-metal is 2.2 Å. In subunit II, the two zincs are separated by 3.7 Å.

Comparison with Phosphotriesterase. Our interest in DHO came as a natural extension of our previous X-ray crystallographic and biochemical analyses of phosphotriesterase (*21*). This dimeric enzyme, isolated from the soil-dwelling bacterium *Pseudomonas diminuta*, catalyzes the detoxification of organophosphate nerve agents such as sarin and soman and pesticides such as parathion and paraoxon. The

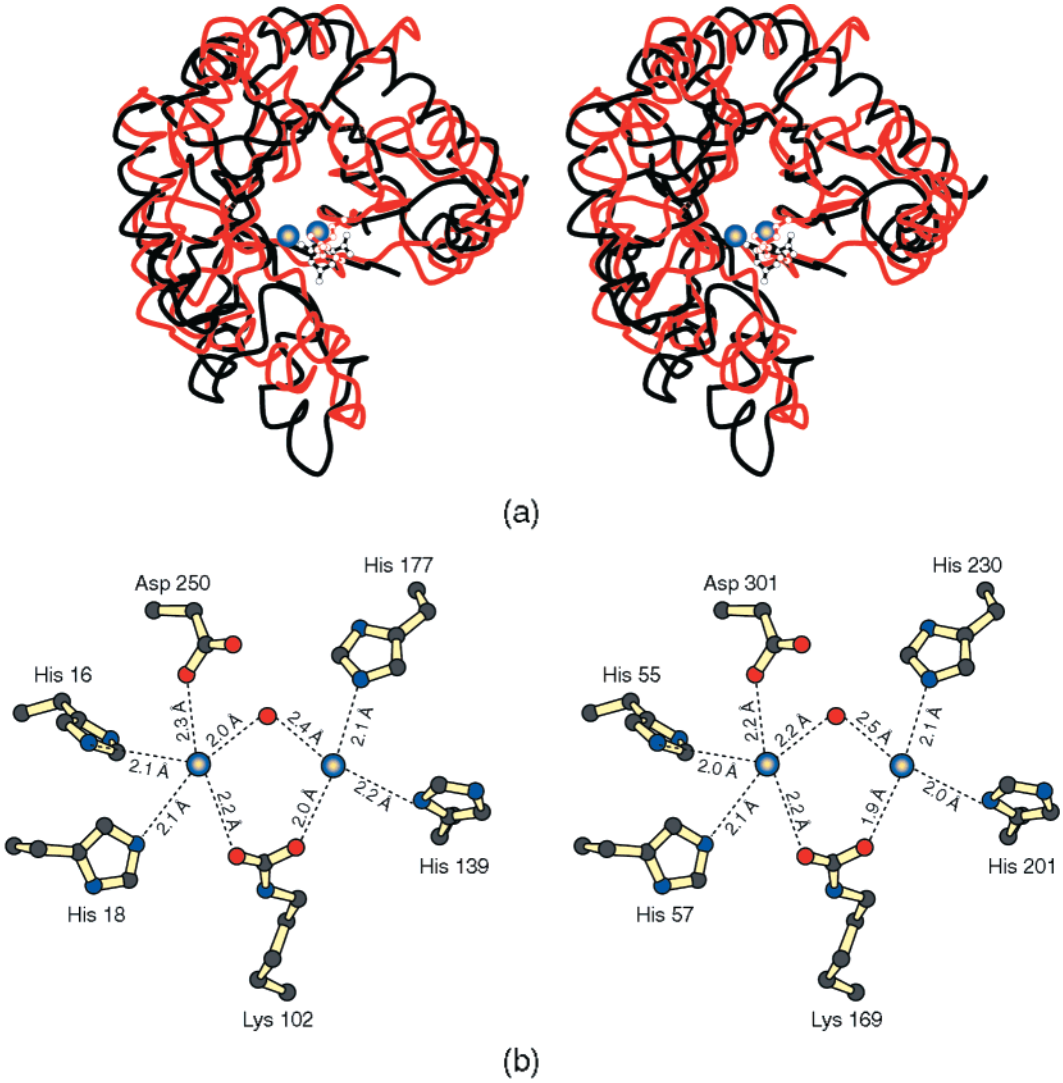

FIGURE 5: Superposition of the TIM barrels observed in DHO and phosphotriesterase. The program employed for the superposition was ALIGN (*29*). Shown in panel a is a superposition of the α-carbons for phosphotriesterase from Phe 51 to Phe 304 (in red) and for DHO from Pro 12 to Pro 253 (black). Dihydroorotate (bound to DHO) and triethyl phosphate (bound to phosphotriesterase) are displayed as ball-and-stick representations. Cartoons are given in panel b that compare the coordination geometries for the binuclear metal centers in DHO (left) and phosphotriesterase (right). The distances quoted for phosphotriesterase are based on the X-ray structure of the enzyme complexed with triethyl phosphate as described in ref *22*.

manner in which phosphotriesterase evolved to catalyze the hydrolysis of phosphotriesters is not well understood, and its actual biological role in the bacterium is unknown.

Shown in Figure 5a is a superposition of the "core" TIM barrels for phosphotriesterase with bound triethyl phosphate (Phe 51−Phe 304) and DHO with bound dihydroorotate (Pro 12−Pro 253) (*22*). The eight strands of β-sheet for these two models correspond with a root-mean-square deviation of 2.9 Å for 72 structurally equivalent α-carbons. The dispositions of the α-helices with respect to the β-strands are significantly different, however. It is clear from these differences why initial attempts to determine the structure of DHO via molecular replacement with phosphotriesterase as the search model were never successful. As indicated in Figure 5a, both phosphotriesterase and DHO bind inhibitors and/or substrates in similar positions with respect to the binuclear metal centers (*22*). The subunit−subunit interactions for these two enzymes, however, are dissimilar, with the buried surface area in phosphotriesterase being larger (~3200 Å^2) and formed by different secondary structural elements (*23*).

Cartoons of the coordination geometries surrounding the binuclear metal centers in DHO and phosphotriesterase are given in Figure 5b. In both enzymes, a carboxylated lysine residue and a hydroxide ion bridge the two metals. It has been proposed that the nucleophile for the hydrolysis reaction catalyzed by phosphotriesterase is, indeed, the metal-bound hydroxide (*24*). The two zincs in phosphotriesterase are separated by 3.5 Å (*22*). As indicated in Figure 5b and in light of experimental error, the binuclear metal centers in DHO and phosphotriesterase are virtually indistinguishable.

Binuclear Metal Center. Prior to this investigation, it was generally believed that the bacterial dihydroorotase would contain a mononuclear metal center within the active site of the protein. This conclusion was based upon the apparent metal stoichiometry for the recombinant hamster DHO (*6*) as well as the enzyme isolated from *E. coli* (*5*). However, the DHO from *Clostridium oroticum* was shown to require two divalent cations for full reconstitution of catalytic activity (*25*). The placement of DHO within the subset of enzymes from the amidohydrolase superfamily that contain a mononuclear metal center was consistent with the failure to identify

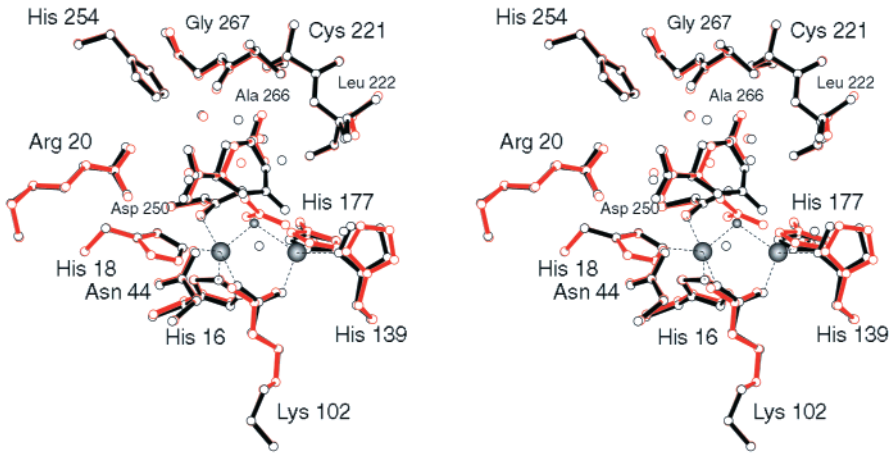

FIGURE 6: Superposition of the two active sites in DHO. Subunit I, with bound dihydroorotate, is drawn in black, while subunit II is depicted in red. The bridging hydroxide, shown as a small gray sphere, is displaced upon the binding of carbamoyl aspartate.

a conserved lysine residue that has served as the hallmark for the bridging ligand in both urease and phosphotriesterase (*9*). In the structure of the *E. coli* DHO, the active site clearly shows the presence of a binuclear metal center that is homologous to that observed in both urease (*11*) and phosphotriesterase (*10*). The bridging ligand is a carbamate functional group, which has been formed through post-translational carboxylation of the ϵ-amino group of Lys 102 with CO_2. Inspection of the entire set of protein sequences for dihydroorotase from available sources reveals for the first time the conservation of a lysine residue immediately after the termination of β-strand 4 within the TIM-barrel motif. Shown in Figure 3 is an alignment of the protein sequences of DHO from *E. coli* and humans. The lysine residue that ultimately functions as the bridging ligand is clearly conserved in this sequence alignment, and thus, we predict that DHO from CAD will likely contain a binuclear metal center.

Reaction Mechanism. The elucidation of the three-dimensional crystal structure of the *E. coli* dihydroorotase in the presence of an equilibrium mixture of the reaction products has unveiled a wealth of information about the molecular mechanism for catalysis by the binuclear metal centers embedded within the amidohydrolase superfamily of enzymes. This unobstructed view of the active site is not distorted by the need to utilize analogues of the substrate and/or product to accurately articulate those protein−ligand interactions that contribute substantially to subsequent catalytic events. The three-dimensional representations of the active site, before and after the chemical transformation, have revealed the distinct contributions for each of the two divalent cations within the binuclear metal center and have clarified the dual role played by Asp 250 in proton abstraction and donation. A superposition of the two active sites with bound substrate and product is presented in Figure 6. The hydrolytic solvent molecule used during the cleavage of dihydroorotate has been identified as the hydroxide that bridges the two divalent cations. The proposed reaction mechanisms for amide bond formation or hydrolysis are summarized in Scheme 2.

In the direction of dihydroorotate hydrolysis, the crystal structure demonstrates that the carbonyl oxygen (O4) of the amide bond about to be cleaved makes a direct molecular contact with the more solvent-exposed β-metal ion. This interaction polarizes the carbonyl−oxygen bond and places

Scheme 2

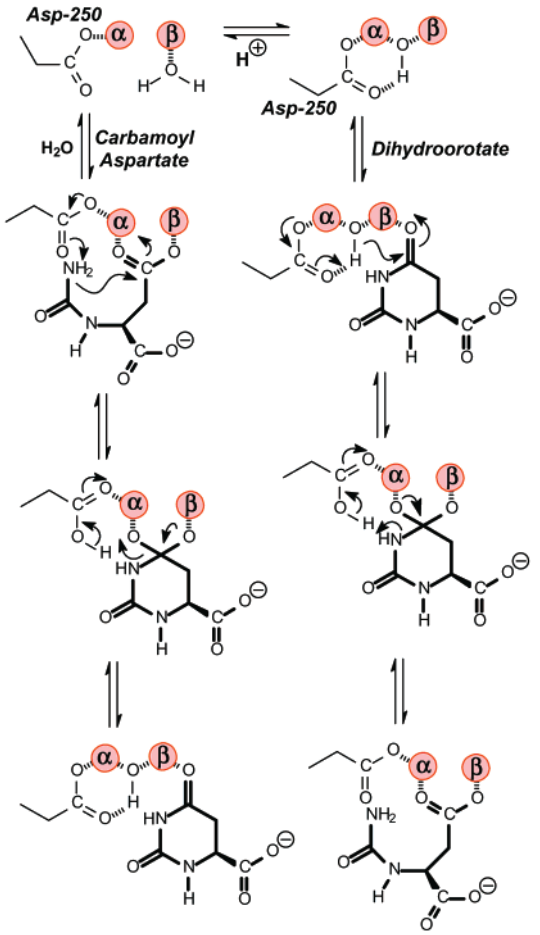

the oxygen of the bridging hydroxide ~2.7 Å away from the carbonyl carbon of dihydroorotate. Nucleophilic attack by the bridging hydroxide on the *re*-face of dihydroorotate is assisted by general base catalysis from the side chain carboxylate of Asp 250. The ensuing tetrahedral intermediate is stabilized via bidentate ligation to both zinc ions of the binuclear metal center. Collapse of this intermediate and cleavage of the carbon−nitrogen bond are assisted by the simultaneous protonation of the amide nitrogen by Asp 250. The carboxylate group of the newly formed carbamoyl aspartate is ligated as a bridge to the α- and β-zinc ions of the binuclear metal center. This coordination scheme, as

found in the actual crystal structure of the bound carbamoyl aspartate, overwhelmingly supports the proposal that the bridging hydroxide, observed in the structure of the bound dihydroorotate, is the direct source for the nucleophile that functions to cleave the carbon−nitrogen bond of dihydroorotate.

In the direction of dihydroorotate biosynthesis, carbamoyl aspartate preferentially binds to a protonated form of the binuclear metal center. In the scheme presented here, the bridging hydroxide group accepts a proton from solvent to form a water molecule that resides primarily on the β-metal ion. This specific proposal is supported by multiple theoretical calculations directed at the homologous binuclear metal center of phosphotriesterase but has not, as yet, been experimentally verified (*26*, *27*). The carboxylate group of the incoming carbamoyl aspartate displaces the water molecule from the β-metal ion and then bridges the two metal ions. The direct molecular contact with the binuclear metal center neutralizes the negative charge and makes the side chain carboxylate carbon more electrophilic. Bond formation is initiated by the abstraction of a proton from N3 of carbamoyl aspartate by the side chain carboxylate of Asp 250. The tetrahedral intermediate is electrostatically stabilized through direct ligation to the binuclear metal center. Collapse of this intermediate via cleavage of the C−O bond is assisted by proton donation from Asp 250. The incipient hydroxide is bridged between the two divalent cations, and the carbonyl oxygen of dihydroorotate is bound directly to the β-metal ion. The molecular interactions between the active site of DHO and the substrates, as revealed in the crystal structure reported in this paper, have provided an unprecedented view of the inner workings of the binuclear metal centers within the amidohydrolase superfamily. An even more complete picture will emerge when the structure of DHO is determined as a function of pH in the absence of substrates and products.

ACKNOWLEDGMENT

We gratefully acknowledge the helpful discussions of Drs. W. W. Cleland and T. C. Terwilliger. Use of the Argonne National Laboratory Structural Biology Center beamlines at the Advanced Photon Source was supported by the U.S. Department of Energy, Office of Energy Research, under Contract W-31-109-ENG-38. We thank Drs. Norma Duke and Ruslan Sanishvili for help with the X-ray data collection.

REFERENCES

1. Washabaugh, M. W., and Collins, K. D. (1984) *J. Biol. Chem. 259*, 3293−3298.
2. Christopherson, R. I., and Jones, M. E. (1979) *J. Biol. Chem. 254*, 12506−12512.
3. Williams, N. K., Manthey, M. K., Hambley, T. W., O'Donoghue, S. I., Keegan, M., Chapman, B. E., and Christopherson, R. I. (1995) *Biochemistry 34*, 11344−11352.
4. Zimmermann, B. H., Kemling, N. M., and Evans, D. R. (1995) *Biochemistry 34*, 7038−7046.
5. Brown, D. C., and Collins, K. D. (1991) *J. Biol. Chem. 266*, 1597−1604.
6. Huang, D. T., Thomas, M. W., and Christopherson, R. I. (1999) *Biochemistry 38*, 9964−9970.
7. Simmer, J. P., Kelly, R. E., Rinker, A. G., Jr., Zimmerman, B. H., Kim, H., and Evans, D. R. (1990) *Proc. Natl. Acad. Sci. U.S.A. 87*, 174−178.
8. Eriksson, A. E., Jones, T. A., and Liljas, A. (1988) *Proteins: Struct., Funct., Genet. 4*, 274−282.
9. Holm, L., and Sander, C. (1997) *Proteins: Struct., Funct., Genet. 28*, 72−82.
10. Benning, M. M., Kuo, J. M., Raushel, F. M., and Holden, H. M. (1995) *Biochemistry 34*, 7973−7978.
11. Jabri, E., Carr, M. B., Hausinger, R. P., and Karplus, P. A. (1995) *Science 268*, 998−1004.
12. Wilson, D. K., Rudolph, F. B., and Quiocho, F. A. (1991) *Science 252*, 1278−1284.
13. Buchbinder, J. L., Stephenson, R. C., Dresser, M. J., Pitera, J. W., Scanlan, T. S., and Fletterick, R. J. (1998) *Biochemistry 37*, 5096−5106.
14. Otwinowski, Z., and Minor, W. (1997) *Methods Enzymol. 276*, 307−326.
15. Terwilliger, T. C., and Berendzen, J. (1999) *Acta Crystallogr. D55*, 849−861.
16. Terwilliger, T. C. (2000) *Acta Crystallogr. D56*, 965−972.
17. Cowtan, K., and Main, P. (1998) *Acta Crystallogr. D54*, 487−493.
18. Tronrud, D. E., Ten Eyck, L. F., and Matthews, B. W. (1987) *Acta Crystallogr. A43*, 489−501.
19. Roussel, A., and Cambillau, C. (1991) in *Silicon Graphics Geometry Partners Directory*, Silicon Graphics, Mountain View, CA.
20. Lee, B., and Richards, F. M. (1971) *J. Mol. Biol. 55*, 379−400.
21. Raushel, F. M., and Holden, H. M. (2000) *Adv. Enzymol. 74*, 51−93.
22. Benning, M. M., Hong, S. B., Raushel, F. M., and Holden, H. M. (2000) *J. Biol. Chem. 275*, 30556−30560.
23. Benning, M. M., Kuo, J. M., Raushel, F. M., and Holden, H. M. (1994) *Biochemistry 33*, 15001−15007.
24. Vanhooke, J. L., Benning, M. M., Raushel, F. M., and Holden, H. M. (1996) *Biochemistry 35*, 6020−6025.
25. Pettigrew, D. W., Bidigare, R. R., Mehta, B. J., Williams, M. I., and Sander, E. G. (1985) *Biochem. J. 230*, 101−108.
26. Zhan, C., de Souza, N., Rittenhouse, R., and Ornstein, R. L. (1999) *J. Am. Chem. Soc. 121*, 7279−7282.
27. Krauss, M. (2001) *J. Chem. Inf. Comput. Sci. 41*, 8−17.
28. Kraulis, P. J. (1991) *J. Appl. Crystallogr. 24*, 946−950.
29. Cohen, G. H. (1997) *J. Appl. Crystallogr. 30*, 1160−1161.

BI010682I